Earth Planets Space, **54**, 1071–1076, 2002

Strain accumulation in and around Ou Backbone Range, northeastern Japan as observed by a dense GPS network

Satoshi Miura, Toshiya Sato, Kenji Tachibana, Yoshimi Satake, and Akira Hasegawa

Research Center for Prediction of Earthquakes and Volcanic Eruptions, Graduate School of Science, Tohoku University, Sendai 980-8578, Japan

(Received December 31, 2001; Revised April 11, 2002; Accepted May 14, 2002)

A dense GPS network was established in 1997 around Ou Backbone Range (OBR), northeastern Japan, by deploying 28 continuous GPS stations to complement the sparse portion of GEONET operated by the Geographical Survey Institute of Japan. The aim of the network is to investigate the present surface deformation and understand the relationship between earthquake occurrence and the deformation process of the island-arc crust. Our GPS data are analyzed using a precise point positioning strategy of GIPSY/OASIS-II. Results of GEONET in daily SINEX files have been supplied by the GSI. Producing grid data of horizontal velocities and taking spatial derivatives, we derived a map of strain rate distribution. The results show that the region between 38.8° and 39.8°N in the OBR experiences notable concentration of east-west contraction. The region coincides with the area of active seismicity, including the focal areas of large earthquakes occurring in 1896 (M7.2), 1900 (M7.0), 1962 (M6.5), 1970 (M6.2), and 1998 (M6.1). Observed strain is larger than can be explained by the total moment release of earthquakes that occurred in the same period as this study. Possible sources of strain concentration may be viscoelastic deformation due to large earthquakes and/or aseismic slip along the deeper extension of the active faults.

1. Introduction

Ou Backbone Range (OBR) runs through the center of the Tohoku District, northeastern Japan, in the north-south direction. It includes many active volcanoes and active faults that have caused disastrous earthquakes. For example, the Senya and Kawafune faults generated the 1896 Riku-u earthquake (M7.2, see Fig. 1) and are of the typical thrust faults in northern Honshu (Matsuda *et al.*, 1980). In 1970, a moderate earthquake with M6.2 occurred south of the Riku-u earthquake (Hasegawa *et al.*, 1974; Hasegawa *et al.*, 1975), and two events with M5.9 and M5.7 took place farther south in 1996 (Umino *et al.*, 1998a). Akita-Komagatake volcano, located north of the 1896 event, erupted in 1970 (e.g. Tanaka *et al.*, 1972), and unrest of Iwate volcano started in 1995 with intermediate-depth tremors (Ueki *et al.*, 1996) followed by notable shallow seismicity (Tanaka *et al.*, 1999) and crustal deformation (Miura *et al.*, 2000). A M6.1 earthquake also occurred about 10 km southwest of the volcano, halfway between Akita-Komagatake and Iwate volcanoes, in 1998 (Umino *et al.*, 1998b; Miura *et al.*, 2000). In addition, shallow intra-plate seismicity shows a concentrated distribution in and around the OBR (Hasegawa *et al.*, 2000), as shown in Fig. 7.

In 1997 and 1998, intensified seismological experiments were carried out to understand the deformation process of the arc crust and its relation to large earthquakes in the northeastern Japan arc. Many temporary seismic stations were deployed to augment the regional seismic networks (Hasegawa and Hirata, 1999). In cooperation with this project, a dense GPS network was also established in 1997 around the OBR to directly observe the deformation of the island-arc crust.

2. Data

The nationwide GPS network, GEONET, composed of about 1000 stations has been established by the Geographical Survey Institute (GSI) (Miyazaki *et al.*, 1997). The network has provided many important observational results, such as measurements of coseismic, post-seismic, inter-seismic, and volcanic deformations, facilitating immense progress to be made in our knowledge of on-going crustal deformation. Baseline lengths of the network, however, sometimes exceed 50 km in the OBR because of its mountainous topography. This separation of GPS stations is not short enough to observe deformation related to the occurrence of M6–7 earthquakes. We utilized 28 continuous GPS stations, taking into account the locations of active faults, to complement the 81 GEONET stations shown in Fig. 2. Nine GPS stations out of 28 were established in 1997.

GPS data sampled every minute are transmitted through the Japanese University Satellite Seismic Telemetry Network System (JUSSTN), a satellite communication system (Urabe, 1996). From some stations, data are transmitted through a public telephone line using a modem. Collected data are analyzed using a precise point positioning (PPP) strategy of GIPSY/OASIS-II (Zumberge *et al.*, 1997), which has been used in many geodetical and geophysical applications (e.g. Ohtani *et al.*, 2000; Shoji *et al.*, 2000; Behrend *et al.*, 2000; Gradinarsky *et al.*, 2000; Becker *et al.*, 2000; Aonashi *et al.*, 2000; Takiguchi *et al.*, 2000; Cardellach *et al.*, 2000). Figure 3 shows an example of time series of ITRF97 coordinates derived at station AKT0. Standard de-

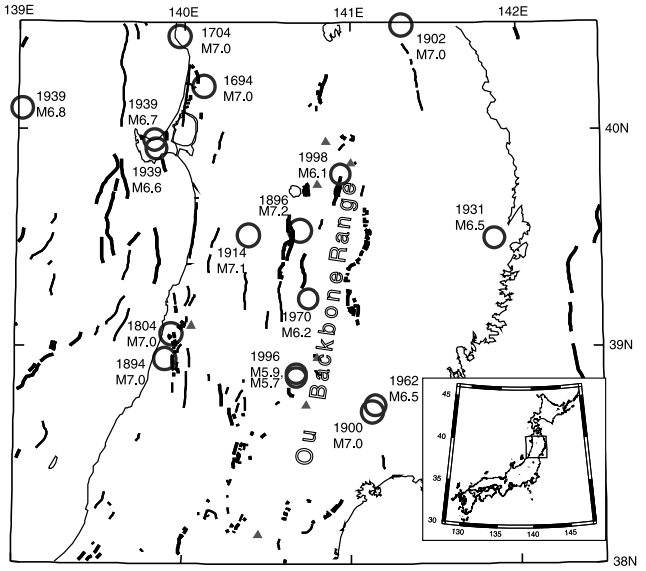

Fig. 1. Distribution of historical earthquakes, active faults, and active volcanoes. Large circles, triangles, and bold lines indicate the epicenters of major events that occurred for the period from 1690 to 2000, active volcanoes, and active faults, respectively. The box in the map of Japan shows the study area.

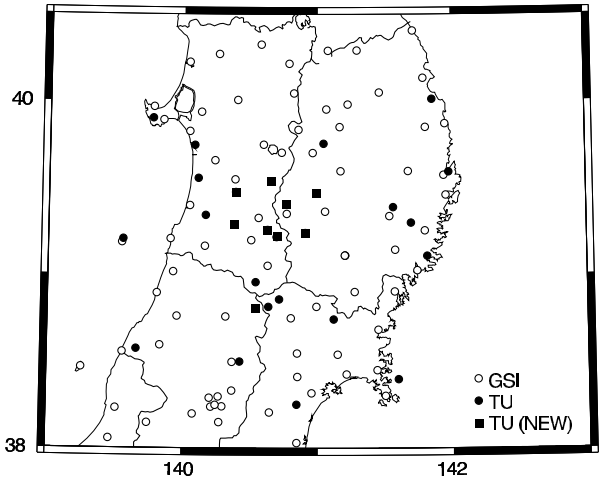

Fig. 2. Map showing GPS stations in the study area. Open and solid circles denote continuous GPS stations operated by Geographical Survey Institute of Japan (GSI) and Tohoku University (TU), respectively. Solid squares are the new sites established by TU for this study.

viations of the north-south, east-west, and elevation components are 4.3 mm, 4.8 mm, and 10.6 mm, respectively. These are slightly larger than those from double-difference-based analyses (DDA) because integer phase biases cannot be resolved by PPP, wherein receiver clock drifts are treated as stochastic parameters (Zumberge *et al*., 1997).

3. Displacement Rate Field

GEONET station positions were estimated by fixing the coordinates at the reference site TSKB, and supplied in daily SINEX (Software Independent Exchange Format) files by the GSI. We independently analyzed the data from TSKB by the PPP method, obtained the velocity of TSKB in ITRF97, and subsequently corrected the velocities at all GEONET

Table 1. Site velocities derived in this study.

Site code	Latitude (deg. in North)	Longitude (deg. in East)	North velocity (mm/yr)	East velocity (mm/yr)
0179	38.02966	140.84399	9.90 ± 0.06	−18.93 ± 0.05
0564	38.05618	139.46168	9.30 ± 0.15	−8.70 ± 0.11
0197	38.14618	139.74225	7.38 ± 0.06	−8.44 ± 0.05
0557	38.14810	140.27114	12.09 ± 0.14	−13.26 ± 0.10
0199	38.19754	140.07757	11.27 ± 0.04	−11.27 ± 0.04
0178	38.20574	140.64285	7.82 ± 0.06	−15.92 ± 0.05
0049	38.23069	139.50957	5.99 ± 0.06	−9.29 ± 0.05
9002	38.23690	140.21236	18.58 ± 0.25	−9.12 ± 0.21
9001	38.23936	140.29257	12.57 ± 0.22	−7.47 ± 0.18
9004	38.24905	140.24387	9.25 ± 0.22	−16.80 ± 0.18
AOB0	38.25161	140.84413	11.79 ± 0.23	−22.97 ± 0.38
0803	38.28898	140.19992	8.64 ± 0.09	−10.24 ± 0.07
9003	38.29675	140.26686	17.54 ± 0.22	−11.08 ± 0.18
0550	38.30119	141.50069	14.50 ± 0.15	−26.98 ± 0.12
0037	38.31749	140.95419	9.37 ± 0.06	−21.19 ± 0.05
0035	38.33103	140.36609	8.25 ± 0.06	−14.77 ± 0.05
EN30	38.39794	141.59768	11.99 ± 0.07	−28.31 ± 0.11
0177	38.41176	140.85137	10.04 ± 0.06	−16.82 ± 0.05
0549	38.42506	141.21291	13.61 ± 0.14	−23.12 ± 0.10
0036	38.44920	141.44117	11.43 ± 0.06	−26.35 ± 0.05
0231	38.46539	139.25335	5.97 ± 0.06	0.39 ± 0.05
0556	38.49677	140.36515	7.61 ± 0.14	−18.36 ± 0.10
MR30	38.49816	140.42237	9.87 ± 0.08	−15.27 ± 0.15
0176	38.53948	141.14754	12.78 ± 0.05	−19.41 ± 0.04
0548	38.54622	140.84788	13.25 ± 0.14	−17.70 ± 0.10
0034	38.55554	139.55580	8.02 ± 0.07	−6.34 ± 0.05
ATM0	38.57223	139.65801	8.49 ± 0.08	−0.73 ± 0.14
0196	38.59404	139.83177	8.31 ± 0.06	−4.65 ± 0.05
0175	38.68270	141.44937	12.21 ± 0.05	−22.10 ± 0.04
WYG0	38.74221	141.11979	11.89 ± 0.07	−22.26 ± 0.11
0174	38.74894	140.80164	12.74 ± 0.05	−13.42 ± 0.04
0033	38.75860	140.31874	9.89 ± 0.05	−9.53 ± 0.04
0195	38.75972	139.95737	7.87 ± 0.06	−5.39 ± 0.05
MGM0	38.80272	140.54243	16.00 ± 0.61	−5.40 ± 1.01
NSG0	38.81473	140.63598	9.84 ± 0.30	−12.85 ± 0.60
0173	38.81534	140.99058	13.26 ± 0.05	−13.85 ± 0.04
GNY0	38.85795	140.71488	10.65 ± 0.12	−14.95 ± 0.18
0032	38.89460	139.80885	8.18 ± 0.06	−4.20 ± 0.05
0545	38.90026	141.27479	15.31 ± 0.15	−21.47 ± 0.10
0172	38.90286	141.57259	11.97 ± 0.04	−18.50 ± 0.03
AKNM	38.95604	140.53976	9.87 ± 0.07	−9.72 ± 0.11
0555	39.01597	139.92749	11.85 ± 0.17	−4.83 ± 0.12
0171	39.02378	141.73985	11.54 ± 0.05	−16.82 ± 0.04
0193	39.05190	140.62958	15.69 ± 0.02	−7.48 ± 0.02
SNR0	39.10717	141.81360	10.18 ± 0.08	−18.39 ± 0.12
0757	39.11047	141.20404	10.50 ± 0.06	−11.91 ± 0.05
0029	39.11063	141.20392	12.62 ± 0.07	−15.92 ± 0.05
MZS3	39.11076	141.20321	15.60 ± 0.17	−14.67 ± 0.11
0546	39.14309	141.57549	13.92 ± 0.18	−15.62 ± 0.13
0192	39.16421	140.16198	11.00 ± 0.04	−4.03 ± 0.03
0194	39.18556	139.54766	8.28 ± 0.04	3.65 ± 0.03
0554	39.19910	140.50669	16.09 ± 0.18	−6.29 ± 0.12
TOB0	39.20453	139.55626	5.88 ± 0.07	0.48 ± 0.11
0191	39.20606	139.90772	9.29 ± 0.04	0.68 ± 0.03
SNN0	39.21671	140.69371	12.37 ± 0.09	−9.24 ± 0.17
GTO0	39.23970	140.90800	13.04 ± 0.12	−11.92 ± 0.19
0170	39.25352	141.79804	10.22 ± 0.05	−12.74 ± 0.04
HRN0	39.25821	140.62729	12.65 ± 0.14	−4.91 ± 0.24
OMN0	39.28874	140.38059	11.47 ± 0.13	−4.12 ± 0.21
KMI0	39.29848	141.69501	8.47 ± 0.32	−14.52 ± 0.56
0190	39.32700	140.55978	11.39 ± 0.04	−0.86 ± 0.03
0169	39.33806	141.53416	11.65 ± 0.05	−11.19 ± 0.04
HOJ0	39.34335	140.16798	9.46 ± 0.08	−2.74 ± 0.15
0544	39.35130	140.76918	11.27 ± 0.07	−10.37 ± 0.06
0168	39.36262	141.05455	13.61 ± 0.04	−8.77 ± 0.03
KGJ0	39.38918	141.56144	9.09 ± 0.10	−15.16 ± 0.14
0031	39.39870	140.04824	8.62 ± 0.07	−3.13 ± 0.05
SAW0	39.40488	140.76840	11.54 ± 0.09	−8.59 ± 0.15
0167	39.45816	141.95526	7.09 ± 0.05	−9.30 ± 0.04
NAM0	39.46811	140.99393	13.68 ± 0.15	−12.05 ± 0.25
NNN0	39.47618	140.39173	10.79 ± 0.12	−4.39 ± 0.18
NKS0	39.53787	140.65337	12.05 ± 0.13	−6.29 ± 0.22
0189	39.54929	140.38662	10.88 ± 0.03	−2.40 ± 0.03
IW30	39.55519	140.11105	3.04 ± 0.07	−4.42 ± 0.11
0028	39.57239	141.93996	6.17 ± 0.07	−10.66 ± 0.05
MYK0	39.59320	141.97684	6.56 ± 0.09	−11.29 ± 0.15
0547	39.59613	141.67529	12.31 ± 0.19	−10.35 ± 0.13
0166	39.59657	141.17211	12.06 ± 0.06	−7.53 ± 0.04
0188	39.65831	140.23421	11.41 ± 0.04	1.24 ± 0.03
0165	39.70109	140.96450	3.29 ± 0.04	−4.81 ± 0.03
0553	39.70268	140.73285	9.15 ± 0.20	−1.36 ± 0.13
AKT0	39.74628	140.08255	10.17 ± 0.11	−3.28 ± 0.17
0187	39.74916	140.59704	10.01 ± 0.04	−1.58 ± 0.03
IWT0	39.75403	141.04525	4.51 ± 0.52	−15.86 ± 0.81
0552	39.82581	140.04472	12.34 ± 0.20	−4.05 ± 0.13
9014	39.83512	140.85573	8.54 ± 0.18	−6.19 ± 0.15
0164	39.84918	141.80385	6.21 ± 0.06	−7.17 ± 0.04
0163	39.85125	141.16486	11.12 ± 0.06	−6.48 ± 0.04
0162	39.86937	141.95054	5.53 ± 0.06	−5.52 ± 0.04
0551	39.89114	139.84893	12.94 ± 0.21	−0.35 ± 0.13
OGA0	39.90175	139.77044	10.07 ± 0.33	−0.89 ± 0.52
0186	39.93606	140.13238	10.05 ± 0.04	0.06 ± 0.03
0543	39.95308	141.06633	17.10 ± 0.07	0.83 ± 0.06
0030	39.96790	139.77615	8.12 ± 0.07	0.48 ± 0.05
0161	39.98058	141.22507	9.94 ± 0.06	−4.81 ± 0.04
0185	40.00688	140.40199	11.07 ± 0.04	−1.23 ± 0.03
FDA0	40.01163	141.85495	3.36 ± 0.07	−7.18 ± 0.10
0798	40.04498	140.82291	17.23 ± 0.09	0.72 ± 0.08
0160	40.04860	141.46195	8.65 ± 0.04	−4.41 ± 0.03
0027	40.13345	141.78910	4.86 ± 0.07	−7.81 ± 0.05
0183	40.21544	140.78733	11.08 ± 0.06	−0.28 ± 0.04
0184	40.22489	140.04228	9.83 ± 0.04	−1.58 ± 0.03
0182	40.27116	140.26366	10.31 ± 0.04	−1.46 ± 0.03
0157	40.29108	141.07648	9.76 ± 0.06	−0.45 ± 0.04
0159	40.29115	141.29369	8.27 ± 0.06	−2.43 ± 0.04
0181	40.32505	140.57735	13.16 ± 0.06	−0.70 ± 0.04
0158	40.40520	141.71314	6.98 ± 0.06	−5.31 ± 0.04

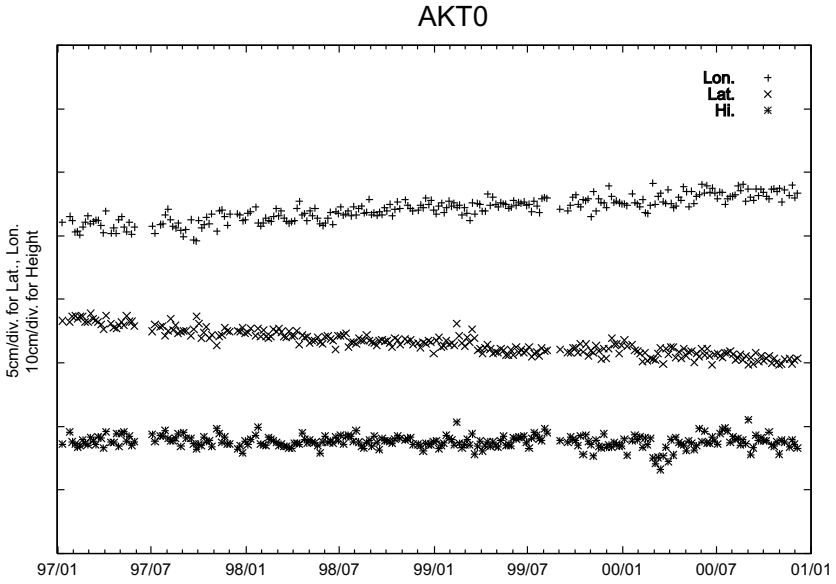

Fig. 3. Time series of variations in coordinates of AKT0 for the period from 1997 to 2000. Longitudinal, latitudinal, and height components are shown from the top. GPS data are analyzed using a precise point positioning technique of GIPSY/OASIS-II.

sites. Horizontal displacement velocities for individual stations have been calculated by fitting linear functions to the time-series of site coordinates. Figure 4 shows a map of the horizontal displacement velocity relative to the plate motion of the North American (NA) Plate estimated in NNR-NUVEL1A (DeMets *et al.*, 1994). North and east velocities determined by this study are listed in Table 1. Some stations co-located by the two institutes (e.g. TOB0 and 0194, MYK0 and 0028, etc.) show similar velocities. Most of the stations show linear trends in displacement. However, an exception is IWT0 located about 10 km southeast of Iwate volcano, which activated in the beginning of 1998 and caused distinct dilatational deformation in a denser local GPS network (Miura *et al.*, 2000). IWT0 was displaced about 2 cm toward the southeast by the activity from February to August, 1998 and also displaced due to a moderate earthquake with $M6.1$ which occurred about 10 km southwest of the volcano. This station was not used for the estimation of strain field because its displacement rate was strongly affected by those activities and shows a different direction from those of the nearby stations (see Fig. 4).

Displacement rates toward the west-northwest are evident at stations along the Pacific coast of Japan. This deformation pattern is likely due to interplate coupling between the Pacific (PA) and NA Plates (Nishimura *et al.*, 2000). In addition, there is a contrast in magnitude of displacement along the Pacific coast: larger in the southern part, while smaller in the northern part. This indicates that the interplate coupling is stronger in the south than in the north during the present observation period. Post-seismic deformation, clearly observed after the 1994 Far Off Sanriku Earthquake ($M7.5$), was attributed to after-slip distribution on the plate boundary by means of a geodetic inversion technique (e.g. Nishimura *et al.*, 2000). Smaller displacements along the northern Pacific coast suggest that the northern part of the plate boundary is still on the way to recovering interplate coupling.

Displacements along the Japan Sea coast are considerably smaller in magnitude and directed to the northwest and the north in the southern and northern area, respectively. Miyazaki (1999) has already derived a similar pattern of displacement rates using GEONET data for the period from 1996 to 1998. He suggested that one possible cause is the existence of a nascent plate boundary between the Eurasian (EU) and NA Plates (Nakamura, 1983; Kobayashi, 1983) near the west coast of the Tohoku District. There may also be a systematic misfit in NNR-NUVEL1A in the boundary zone of the NA Plate. The OBR lies halfway between the two coasts and shows a transitional pattern between the different deformation characteristics.

Shown in Fig. 5 are longitudinal profiles of east-west site velocities in the three regions indicated in the map. Overall strain rates in the study area increase from north to south. The site velocities in the central region are more scattered than the other regions, implying greater inhomogeneity in the strain field in this region.

4. Strain Rate Field

Research to derive continuous deformation fields from sparsely distributed geodetic data has been performed by Miura *et al.* (1989) and Sato *et al.* (1993). Gridded data of horizontal site velocities were produced with GMT (General Mapping Tools, Wessel and Smith, 1991). We used a 64×64 grid with an interval of about 4 km, a spacing related to the station separation in the study area. The strain rate field is determined by taking spatial derivatives of the gridded site velocities. The distribution of principal strain rates of each grid point is shown in Fig. 6, which is characterized by east-west contraction and small north-south strain rates except for some localized regions. This agrees well with the fact that the typical focal mechanism of shallow intraplate earthquakes is dominated by east-west compression (Hasegawa *et al.*, 1994; Kosuga *et al.*, 1996). Tada (1986) demonstrated east-west contraction in and around the OBR, together with north-south extension around the Kitakami Mountains, using

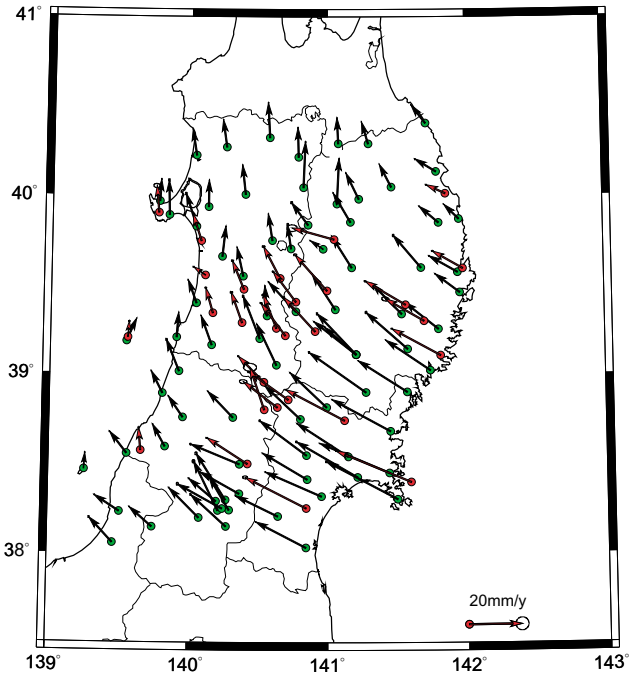

Fig. 4. Horizontal displacement velocity relative to the motion of the North American Plate obtained at each continuous GPS station. Red and black arrows indicate horizontal velocities at the site of Tohoku University and GSI, respectively.

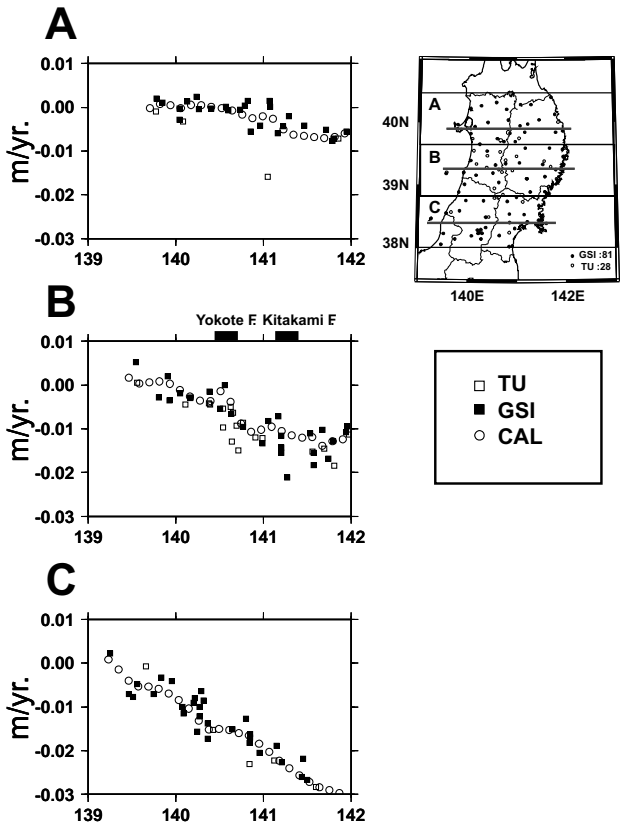

Fig. 5. Longitudinal profiles of east-west displacement rates in three regions shown in the map (A, B, and C). Open and solid squares indicate observed displacement rates at stations of Tohoku University and GSI, respectively. Open circles denote interpolated rates along lines shown in each region by means of the method described in Section 4.

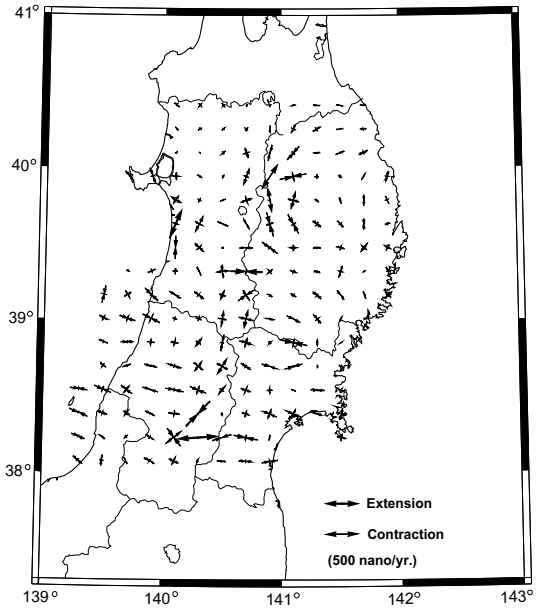

Fig. 6. Distribution of horizontal principal-strain rate.

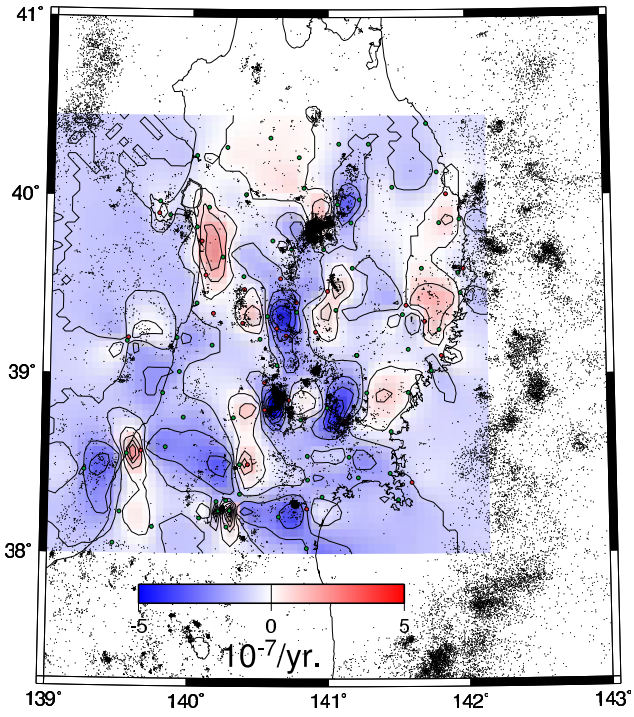

Fig. 7. Distribution of horizontal east-west strain rate. Contour interval is 100 ppb/yr. Dots indicate epicenters of microearthquakes which occurred for the period from 1997 to 2000 with depth ≤40 km.

triangulation and trilateration surveys conducted by the GSI. The former coincides with the present study, while the latter does not. This may be due to the difference in the observation period and/or the accuracy of the conventional surveys.

Figure 7 shows the east-west strain rate field. The region between 38.8° and 39.8°N in the OBR exibits notable concentration of east-west contraction, and coincides with the area of active seismicity. It also includes the focal areas of large earthquakes such as the 1896 (M7.2), 1900 (M7.0),

1962 (M6.5), 1970 (M6.2), and 1998 (M6.1) events shown in Fig. 1, and lies near the source region of the M5.9 and M5.7 sequence in 1996. Concentration of shallow seismicity, high topography, and relatively large contractional deformation of the crust in the OBR was examined by Hasegawa *et al.* (2000) using the strain distribution in the direction of plate convergence derived by triangulation/trilateration in the last 100 years. They suggested this feature was caused by a horizontally inhomogeneous distribution of temperature within the crust. We cannot find any clear correlation between the east-west strain rate distribution and the other major events which occurred outside the OBR.

The total moment release calculated from magnitudes of earthquakes that occurred in the same period of this study is about 2.4×10^{16} Nm, which corresponds to M_w4.9 and generates strain release of about 25 ppb/yr in the area of 100 km^2, even if we assume that all the earthquakes have occurred at the same location with the same focal mechanism. The observed strain, however, is a few hundred parts per billion per year over a few hundred square kilometers, and, thus, it is due primarily to aseismic processes.

5. Discussion

Sagiya *et al*. (2000) investigated the secular deformation field all over the Japanese islands using GEONET data. They reported detailed characteristics of present-day strain distribution and the existence of the Niigata-Kobe Tectonic Zone with strain rates larger than 0.1 ppm/yr, where six large earthquakes with M7 or larger have occurred in the last 200 years. They estimated the contractional strain in and around the OBR and showed it has rather broad distribution. It is obvious that this disagreement is due to the difference in the number of stations used. The deployment of dense GPS networks is very effective for detailed deformation studies.

Possible sources of the strain concentration might be viscoelastic deformation due to large earthquakes and/or aseismic slip along the deeper extension of the active faults. Thatcher *et al.* (1980) derived transient crustal subsidence from leveling data conducted by the GSI in the source region of the 1896 Riku-u earthquake. They interpreted it as postseismic rebound due to a viscoelastic response of the mantle to coseismic deformation. Komatsubara and Awata (2001) suggested the occurrence of pre-seismic slip on a horizontal detachment fault at the base of the seismogenic layer (13 km in depth) prior to the 1970 event (M6.2). Sagiya *et al.* (2002) also proposed a model of horizontal detachment to explain the observed concentrated deformation around the East Matsumoto-Basin Fault. It is a task for future work to construct an adequate model to interpret the observed strain field in the OBR taking into account the detailed crustal structure obtained by the seismic experiments and other geophysical results (e.g. Hirata *et al.*, 1999; Sato *et al.*, 2002; Nakajima *et al.*, 2001).

6. Conclusions

Three-year observations of crustal deformation by a dense GPS network in and around the OBR reveals a distinct concentration in east-west strain. This feature agrees with focal mechanisms and hypocenter distributions of shallow intraplate earthquakes and with the locations of active faults. The observed strain is too much large to be explained by the total moment release of the earthquakes occurring in the same period. This suggests the existence of an aseismic process causing the strain accumulation in the OBR.

Acknowledgments. The authors are grateful to Keiji Kasahara, Kazushige Obara, and Teruyuki Kato who provided GPS instruments. We thank the Geographical Survey Institute for permitting the use of GEONET data. We also thank two reviewers, Wayne Thatcher and Takeshi Sagiya for their useful comments and criticisms, and Aaron D. Sweeney for his critical reading of the manuscript.

References

Aonashi, K., Y. Shoji, R. Ichikawa, and H. Hanado, Estimation of PWC gradients over the Kanto Plain using GPS data: Validation and possible meteorological implications, *Earth Planets Space*, **52**, 907–912, 2000.

Becker, M., E. Reinhart, S. B. Nordin, D. Angermann, G. Michel, and C. Reigber, Improving the velocity field in South and South-East Asia: The third round of GEODYSSEA, *Earth Planets Space*, **52**, 1113–1116, 2000.

Behrend, D., L. Cucurull, J. Vilà, and R. Haas, An inter-comparison study to estimate zenith wet delays using VLBI, GPS, and NWP models, *Earth Planets Space*, **52**, 691–694, 2000.

Cardellach, E., D. Behrend, G. Ruffini, and A. Rius, The use of GPS buoys in the determination of oceanic variables, *Earth Planets Space*, **52**, 721–726, 2000.

DeMets, C., R. C. Gordon, D. F. Argus, and S. Stein, Effect of recent revisions to the geomagnetic reversal time scale on estimates of current plate motion, *Geophys. Res. Lett.*, **21**, 2191–2194, 1994.

Gradinarsky, L. P., R. Haas, G. Elgered, and J. M. Johansson, Wet path delay and delay gradients inferred from microwave radiometer, GPS and VLBI observations, *Earth Planets Space*, **52**, 695–698, 2000.

Hasegawa, A. and N. Hirata, An introduction to the transect of northeastern Japan: deformation of island-arc and crustal activity, *Chikyu*, Supl. **27**, 5–11, 1999 (in Japanese).

Hasegawa, T., S. Hori, T. Hasegawa, K. Kasahara, S. Horiuchi, and J. Koyama, On the focal mechanism of the Southeastern Akita Earthquake in 1970, *J. Seismol. Soc. Jpn.*, **27**, 302–312, 1974 (in Japanese with an English abstract).

Hasegawa, A., K. Kasahara, T. Hasegawa, and S. Hori, On the focal mechanism of the Southeastern Akita Earthquake in 1970 (2), *J. Seismol. Soc. Jpn.*, **28**, 141–151, 1975 (in Japanese with an English abstract).

Hasegawa, A., S. Horiuchi, and N. Umino, Seismic structure of the northeastern Japan convergent margin: A synthesis, *J. Geophys. Res.*, **99**, 22,295–22,311, 1994.

Hasegawa, A., A. Yamamoto, N. Umino, S. Miura, S. Horiuchi, D. Zhao, and H. Sato, Seismic activity and deformation process of the overriding plate in the northeastern Japan subduction zone, *Tectonophys.*, **319**, 225–239, 2000.

Hirata, N., H. Hagiwara, M. Matsubara, and H. Sato, Three dimensional seismic structure and crustal activity in northeastern Japan arc derived by integrated seismic experiment in the North-eastern Honshu, *Chikyu*, Supl. **27**, 22–27, 1999 (in Japanese).

Kobayashi, Y., Initiation of subduction of plates, *Chikyu*, **5**, 510–514, 1983 (in Japanese).

Komatsubara, T. and Y. Awata, Analyses of Pre-, Co-, and Post-seismic vertical crustal movement on the Southeastern Akita earthquake of 1970—An evidence of pre-slip at the base of the seismogenic layer—, *J. Seismol. Soc. Jpn.*, **54**, 33–44, 2001 (in Japanese with an English abstract).

Kosuga, M., T. Sato, A. Hasegawa, T. Matsuzawa, S. Suzuki, and Y. Motoya, Spatial distribution of intermediate-depth earthquakes with horizontal or vertical nodal planes beneath northeastern Japan, *Phys. Earth Planet. Int.*, **93**, 63–89, 1996.

Matsuda, T., H. Yamazaki, T. Nakata, and T. Imaizumi, The surface faulting associated with Riku-u earthquake of 1896, *Bull. Earthquake Res. Inst. Tokyo Univ.*, **55**, 795–855, 1980 (in Japanese with an English abstract).

Miura, S., H. Ishii, and A. Takagi, Migration of vertical deformations and coupling of island arc plate and subducting plate, *Geophys. Monograph*, **49**/IUGG ser. 4, 125–138, 1989.

Miura, S., S. Ueki, T. Sato, K. Tachibana, and H. Hamaguchi, Crustal deformation associated with the 1998 seismo-volcanic crisis of Iwate Volcano, Northeastern Japan, as observed by a dense GPS network, *Earth*

Planets Space, **52**, 1003–1008, 2000.

Miyazaki, S., Interseismic crustal deformation in and around the Japan islands as deduced from GPS observations, Doctor Thesis, Tohoku University, 129 pp., 1999.

Miyazaki, S., T. Saito, M. Sasaki, Y. Hatanaka, and Y. Iimura, Expansion of GSI's nationwide GPS array, *Bull. Geogr. Surv. Inst.*, **43**, 23–34, 1997.

Nakajima, J., T. Matsuzawa, A. Hasegawa, and D. Zhao, Seismic imaging of arc magma and fluids under the central part of northeastern Japan, *Tectonophys.*, **341**, 1–17, 2001.

Nakamura, K., Possible nascent trench along the eastern Japan Sea as the convergence boundary between Eurasian and North American plates, *Bull. Earthquake Res. Inst. Univ. Tokyo*, **58**, 711–722, 1983 (in Japanese with English abstract).

Nishimura, T., S. Miura, K. Tachibana, K. Hashimoto, T. Sato, S. Hori, E. Murakami, T. Kono, K. Nida, M. Mishina, T. Hirasawa, and S. Miyazaki, Distribution of seismic coupling on the subducting plate boundary in northeastern Japan inferred from GPS observations, *Tectonophys.*, **323**, 217–238, 2000.

Ohtani, R., N. Koizumi, N. Matsumoto, and E. Tsukuda, Preliminary results from permanent GPS array by the Geological Survey of Japan in conjunction with groundwater-level observations, *Earth Planets Space*, **52**, 663–668, 2000.

Sagiya, T., S. Miyazaki, and T. Tada, Continuous GPS array and present-day crustal deformation of Japan, *Pure Appl. Geophys.*, **157**, 2303–2322, 2000.

Sagiya, T., T. Nishimura, Y. Iio, and T. Tada, Crustal deformation around the northern and central Itoigawa-Shizuoka Tectonic Line, *Earth Planets Space*, **54**, this issue, 1059–1063, 2002.

Sato, T., S. Miura, K. Tachibana, Representation for horizontal crustal deformation by means of Chebychev polynomials, *J. Geod. Soc. Jpn.*, **39**, 263–274, 1993 (in Japanese with an English abstract).

Sato, H., N. Hirata, T. Iwasaki, M. Matsubara, and T. Ikawa, Deep seismic reflection profiling across the Ou Backbone Range, northern Honshu island, Japan, *Tectonophys.*, 2002 (in press).

Shoji, Y., H. Nakamura, K. Aonashi, A. Ichiki, H. Seko, and Members of GPS/MET Japan Summer Campaign 1997 in Tsukuba, Semi-diurnal and diurnal variation of errors in GPS precipitable water vapor at Tsukuba, Japan caused by site displacement due to ocean tidal loading, *Earth Planets Space*, **52**, 685–690, 2000.

Tada, T., Horizontal crustal strain in the northeastern Japan arc and its relation to the tectonics, *J. Seismol. Soc. Jpn.*, **39**, 257–265, 1986 (in Japanese with an English abstract).

Takiguchi, H., T. Kato, H. Kobayashi, and T. Nakaegawa, GPS observations in Thailand for hydrological applications, *Earth Planets Space*, **52**, 913–919, 2000.

Tanaka, K., M. Kasahara, S. Hori, Z. Suzuki, and A. Takagi, Research on Akita-Komagatake (I)—Summary of its eruptions in 1970–1971, *Sci. Rep. Tohoku Univ.*, **21**, 61–75, 1972.

Tanaka, S., H. Nakamichi, H. Hamaguchi, and S. Ueki, The 1998 seismic activity of Mount Iwate, *Chikyu*, **21**, 273–279, 1999 (in Japanese).

Thatcher, W., J. B. Rundall, T. Kato, and T. Matsuda, Lithospheric loading by the 1896 Riku-u earthquake, northern Japan: Implications for plate flexure and asthenospheric rheology, *J. Geophys. Res.*, **85**, 6429–6435, 1980.

Ueki, S., Y. Morita, and H. Hamaguchi, On the volcanic tremor observed at Iwate Volcano in September and October, 1995, *Tohoku J. Natural Disas. Sci.*, **32**, 285–292, 1996 (in Japanese).

Umino, N., T. Matsuzawa, S. Hori, A. Nakamura, A. Yamamoto, A. Hasegawa, and T. Yoshida, 1996 Onikobe earthquakes and their relation to crustal structure, *J. Seismol. Soc. Jpn.*, **51**, 253–264, 1998a (in Japanese with an English abstract).

Umino, N., T. Okada, A. Nakamura, J. Nakajima, T. Sato, S. Hori, T. Kono, K. Nida, S. Ueki, T. Matsuzawa, A. Hasegawa, and H. Hamaguchi, Aftershock distribution for the M6.1 earthquake of 3 September 1998 in Shizukuishi, Iwate prefecture, northeastern Japan, *Active Fault Res.*, **17**, 1–8, 1998b (in Japanese with an English abstract).

Urabe, T., Basic design of an earthquake telemetering system utilizing a communication satellite, *Programme Abstr. Seismol. Soc. Jpn.*, P22, 1996 (in Japanese).

Wessel, P. and W. H. F. Smith, Free software helps map and display data, *Abstr. EOS Tran. Am. Geophys. Union*, **72**, 445–446, 1991.

Zumberge, J. F., M. B. Heflin, D. C. Jefferson, M. M. Watkins, and F. H. Webb, Precise point positioning for the efficient and robust analysis of GPS data from large networks, *J. Geophys. Res.*, **102**, 5005–5017, 1997.

S. Miura (e-mail: miura@aob.geophys.tohoku.ac.jp), T. Sato, K. Tachibana, Y. Satake, and A. Hasegawa